AIP | Applied Physics Letters

Experimental realization of a variable index transmission line metamaterial as an acoustic leaky-wave antenna

Christina J. Naify, Christopher N. Layman, Theodore P. Martin, Michael Nicholas, David C. Calvo, and Gregory J. Orris

Citation: Applied Physics Letters **102**, 203508 (2013); doi: 10.1063/1.4807280
View online: http://dx.doi.org/10.1063/1.4807280
View Table of Contents: http://scitation.aip.org/content/aip/journal/apl/102/20?ver=pdfcov
Published by the AIP Publishing

Experimental realization of a variable index transmission line metamaterial as an acoustic leaky-wave antenna

Christina J. Naify,[1,a)] Christopher N. Layman,[1] Theodore P. Martin,[2] Michael Nicholas,[2] David C. Calvo,[2] and Gregory J. Orris[2]
[1]*National Research Council, Washington, DC 20001, USA*
[2]*U.S. Naval Research Laboratory, Washington, DC 20375, USA*

(Received 4 January 2013; accepted 24 April 2013; published online 23 May 2013)

Development and experimental realization of an acoustic leaky wave antenna are presented. The antenna uses a one-dimensional composite right/left hand transmission line approach to tune radiation angle continually from backfire-to-endfire, including broadside, as a function of input frequency. An array of acoustically loaded membranes and open channels form a structure with negative, zero, or positive refractive index, depending on excitation frequency. The fast-wave radiation band of the antenna is determined using acoustic circuit analysis. Based on the designs specified by circuit and finite element analysis, an acoustic leaky wave antenna was fabricated, and the radiation direction measured at discrete frequencies. © *2013 AIP Publishing LLC*. [http://dx.doi.org/10.1063/1.4807280]

Manipulation of sound waves using acoustic metamaterials has expanded significantly in recent years. Acoustic metamaterials are a class of materials that use sub-wavelength structures to achieve effective bulk properties under acoustic excitation. Unusual effective physical properties, including negative effective bulk modulus,[1] negative effective mass density,[2,3] and negative index[4] have been achieved using metamaterials. Additionally, the development of structures based on transformation acoustics has resulted in designs for scattering reduction[5,6] and sound focusing.[7,8] However, experimental validation of much of the theoretically predicted results is rare.

Leaky wave antennas (LWA) as directional sources have been investigated thoroughly in the electromagnetic spectrum.[9–11] In a typical periodic LWA, a 1-D guiding structure is loaded with inductance (mass) or capacitance (compliance) elements to control the propagation of the guided wave. When only one mass or compliance element has a positive effective value, an open stopband exists, turning the LWA into a standing-wave type of antenna which does not allow for broadside radiation. LWAs with continuous backfire-to-endfire scanning capabilities have been developed using transmission line (TL) metamaterial structures with negative index below a transition frequency. The radiated direction is controlled by varying the index of refraction, which is a function of the input frequency.[12,13]

Recently, a geometry for an acoustic TL structure with continuously varying positive to negative refractive index has been proposed.[14,15] This TL structure was envisioned to use membranes within a pipe-like structure, and open shunt masses which port directly to the surrounding medium. By designing the geometry and material properties of the membrane and shunt elements so that the transition from positive to negative values of the effective parameters occur at the same frequency (the transition frequency, f_0), defined as a balanced condition,[13,14] continuous scanning is possible from left hand to right hand propagation regions. Unlike resonant-based structures in which negative values exist over a narrow bandwidth,[2] the negative parameters of the TL structure occurred below the transition (and resonance) frequency.[16–21] The acoustic behavior of the TL structure was evaluated using both acoustic circuit analysis and full-wave simulation to understand the role of the geometry and material parameters on the transmission profile. It was concluded that, consistent with the electromagnetic LWAs, backward propagation both within the TL structure and for the radiated wave occurred for negative index values while forward propagation occurred for positive index values.

In this report, an acoustic leaky wave antenna for airborn operation is designed, fabricated, and measured. Acoustic circuit analysis was used as a design tool to determine the geometry of the unit cell required to ensure a continuously scanning backfire-to-endfire LWA. The calculated acoustic mass and compliance of the unit cell were then used to determine the radiation profile of an 8-celled LWA at discrete frequencies. Radiation profiles of the structure at discrete frequencies were confirmed using finite element method (FEM) simulations. The measured radiation patterns of the LWA were consistent with the predicted directionality.

The symmetric unit cell consisted of a single membrane, waveguide section, and half of a shunt length at either end as shown in Fig. 1. Membranes were mounted in a circular, rigid waveguide while shunts were achieved using radial slits around the waveguide circumference. Consistent with the acoustic circuit theory, no tension was applied across the membranes. The membranes thus behaved as plates in the scientific sense in that their behavior was dominated by bending stiffness.

Acoustic mass and compliance of each element (membrane, shunt, and waveguide) in the TL were evaluated independently and used to calculate the mass and compliance of the unit cell. The calculated acoustic mass and compliance of the unit cell incorporates radiation loads for the radial shunts, waveguide between membranes, and membrane

[a)]Electronic mail: christina.naify.ctr@nrl.navy.mil

elements. Full mathematical details of the acoustic circuit analysis are described elsewhere and will not be given in detail here.[14,15,22] Figure 1(c) shows a schematic of the acoustic lumped element model for the symmetric unit cell.

Propagation of the acoustic waves through the periodic structure is characterized using Bloch theory by incorporating the acoustic circuit elements defined by the unit cell. The Bloch propagation constant γ_B is defined as

$$\gamma_B = \operatorname{arccosh}\left(1 - \frac{X^2}{2}\right) = \alpha + i\beta_B, \tag{1a}$$

$$X = \frac{\omega}{\omega_R} - \frac{\omega_L}{\omega} \tag{1b}$$

for angular frequency ω, with the right-hand ω_R and left-hand ω_L cutoff frequencies defined as

$$\omega_R = \frac{1}{\sqrt{(M_{shunt} + M_{TL})(C_{shunt} + C_{TL})}}, \tag{2a}$$

$$\omega_L = \frac{1}{\sqrt{M_{TL} C_{mem}}}. \tag{2b}$$

The real component of the propagation constant is the leakage factor α, while the imaginary component is the phase constant β_B, or change in phase per unit length. The acoustic mass (M) and compliance (C) of the shunt, membrane (mem), and TL unit cell are defined by the geometry and material properties through boundary conditions and thin plate theory.[14]

The right and left cutoff frequencies define the range of the pass bandwidth. At frequencies less than the ω_L, and greater than the ω_R, a band gap exists and no propagation occurs. In the general case, the circuit analysis also produces a band-gap between the positive and negative index regions. This band gap results from a geometric design in which only one of the effective parameters (density or modulus) is positive, while the other is negative. The resulting wavenumber is then imaginary and does not propagate through the tube, or radiate into the surrounding area. By properly tuning the effective properties of the acoustic elements, the band gap is closed and a continuous transition from negative to positive index is achieved. The target transition frequency for the LWA geometry reported here occurs at 925 Hz.

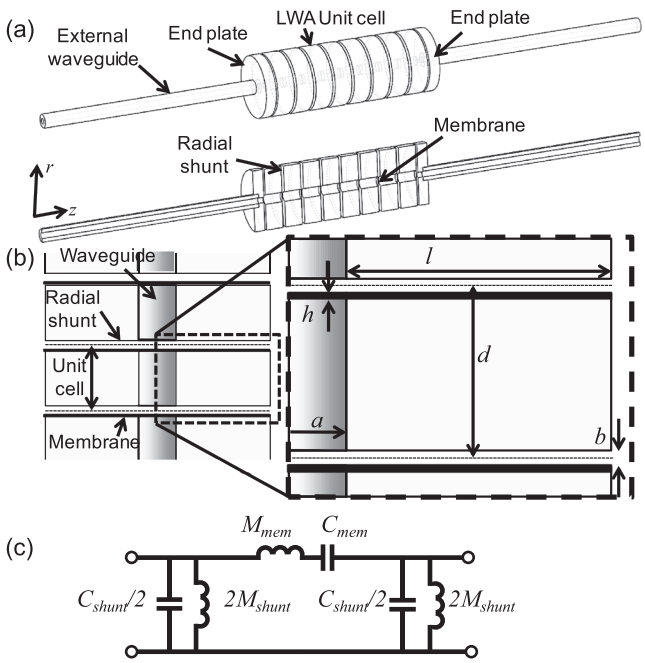

FIG. 1. (a) Axisymmetric LWA Structure (top), section cut of LWA structure (bottom). (b) Detail of acoustic TL metamaterial unit cell showing membranes, shunts and acoustic waveguide outlet (not to scale). (c) Lumped element model for the symmetric unit cell.

Eight LWA unit cells were fabricated using a three-dimensional rapid prototyping technique using UV-cured polymer deposition. The material properties of the polymer were density $\rho_m = 1180\,\mathrm{kg/m^3}$, Young's modulus $E_m = 2\,\mathrm{GPa}$, and Poisson's ratio $\nu = 0.34$. The proprietary material properties reported were obtained from the polymer distributer. Due to resolution limitations of the prototyping technique, a commercially available polymer thin film with similar material properties to the prototyping material was used for the membranes. The surrounding fluid medium for the TL structure was air with density $\rho = 1.188\,\mathrm{kg/m^3}$, bulk modulus $K = 137.4\,\mathrm{kPa}$, and sound speed $c = 343\,\mathrm{m/s}$. The details of the unit cell geometry are given in Table I. The wavelength of the transition frequency was around ten times the size of the unit cell so that the effective medium theory could be implemented.

Each cylindrical LWA unit cell was constructed with an outer radius of 58.01 mm, inner radius of 9.06 mm, and height of 33.14 mm. The unit cells were separated using pins of height 0.86 mm to create the axisymmetric shunts. At either end of the LWA structure, spacers with half-shunt widths of 0.43 mm were connected to end plates so that each unit cell had a half-shunt width at either end. Additionally, at the incident and termination ends of the LWA, external waveguides (also fabricated using the rapid prototype material) of radius 5.54 mm and length 0.43 m were connected to each end plate to ensure a plane wave was incident on the structure and to minimize the effects of reflection within the waveguide.

Figure 2(a) shows the product $\beta_B d$ of the calculated Bloch parameter times the lattice constant as a function of frequency for the fabricated LWA. The continuous scanning condition requires the resonance frequencies of the shunt and membrane elements to be equal. The negative index region, corresponding to the frequency range of the dispersion with phase and group velocities having opposite sign, occurs below the transition frequency and resulted in negative propagation. The transition as well as right and left-hand cutoff frequencies are indicated in Fig. 2(a). Using circuit analysis, the effective medium parameters (density and modulus) were calculated. It can be seen in Fig. 2(b) that the transition

TABLE I. Geometric parameters of the TL leaky wave antenna.

Feature	Dimension (m)
Membrane thickness (h)	125×10^{-6}
Membrane radius (a)	9.06×10^{-3}
Lattice constant (d)	34×10^{-3}
Radial shunt width (b)	0.86×10^{-3}
Radial shunt length (L)	48.95×10^{-3}

frequencies for the effective density and modulus occur at the same frequency value.

The Bloch parameters are used to calculate the radiation angle of the LWA. Radiation of the LWA occurs in the fast-wave band of the dispersion diagram in which the phase velocity of the TL was greater than the phase velocity of the surrounding fluid. For reference, the propagation of the acoustic waves in air is indicated in Fig. 2(a) as the "Light lines." Excitation at frequencies in the left-hand region between f_1 and f_0 results in backfire radiation (toward the source), while excitation at frequencies in the right-hand region between f_0 and f_2 results in endfire radiation (toward the termination). Outside of the radiation bandwidth, waves propagate through the waveguide without radiation.

The radiation angle for a periodic LWA is[12]

$$\theta_0 = \arcsin(\beta_B(\omega)/k_0), \tag{3}$$

where β_B and k_0 are the propagation constant and wavenumber in air at the desired frequency, respectively. The phase and magnitude functions of the radiation pattern of the N-celled array-type LWA are designated $\xi_{\theta n}$ and $I_{\theta n}$, respectively

$$\xi_{\theta n} = -(n-1)k_0 d\sin(\theta_0), \tag{4a}$$

$$I_{\theta n} = I_0 e^{-\alpha(n-1)d}. \tag{4b}$$

The radiation pattern of the LWA with N cells is then

$$R(\theta) = \sum_{n=1}^{N} I_{\theta n} e^{i(n-1)k_0 d\sin(\theta)+i\xi_{\theta n}}. \tag{5}$$

Figure 3 shows the calculated radiation pattern for the LWA evaluated at 800 Hz, 925 Hz, and 1000 Hz. Backfire radiation, indicated by a negative radiation angle of -67.1°, is seen at 800 Hz, while endfire radiation at an angle of 47.5° is seen at 1000 Hz. Broadside radiation, where the refractive index and radiation angle are approximately zero, occurs at the transition frequency 925 Hz.

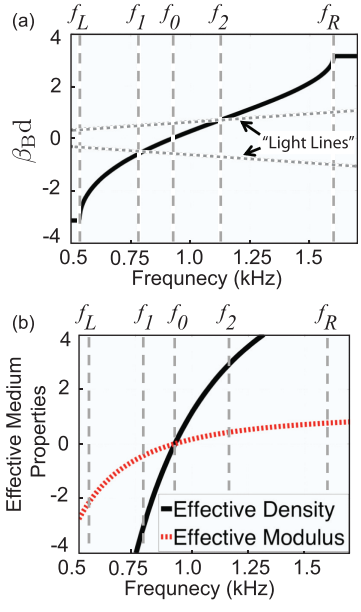

FIG. 2. (a) Phase constant times lattice constant calculated using Bloch theory for implemented geometry. The antenna operates between backfire f_1 and endfire f_2 frequencies with zero-index frequency occurring at 925 Hz (f_0). (b) Effective parameters calculated using acoustic circuit analysis. Matched condition of zero effective density and modulus occurs at 925 Hz.

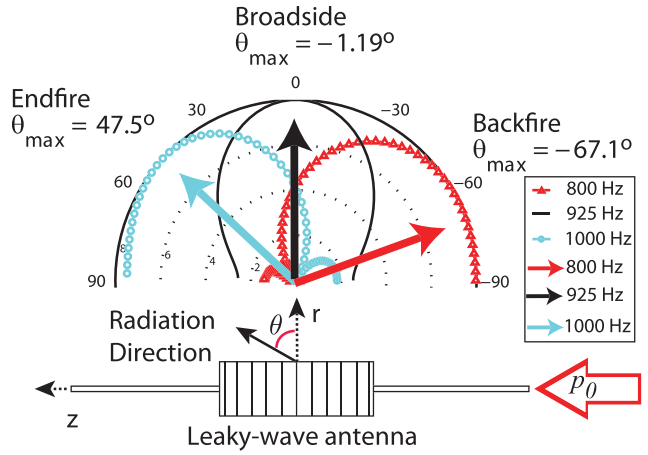

FIG. 3. Radiation pattern of an eight-cell LWA calculated using equivalent circuit analysis for backfire-to-endfire scanning. Backfire (f = 800 Hz, radiation angle = -67.1°) corresponds to negative refractive index, broadside (f_0 = 925 Hz, radiation angle = -1.19°) corresponds to zero index, and endfire (f = 1000 Hz, radiation angle = 47.5°) corresponds to positive refractive index. Arrows indicate the direction of maximum radiation as calculated by Eq. (5). Bottom: schematic of radiation direction with respect to incident pressure.

In addition to acoustic circuit analysis, modeling using the FEM in COMSOL MULTIPHYSICS software was also performed. The axisymmetric structure was excited using an incident plane wave with input pressure of 1 Pa. A perfectly matched layer was specified at the termination to prevent reflection, and radiation conditions were imposed on the exterior boundaries. Figures 4(a)–4(c) show the predicted sound pressure levels (SPL) for the LWA at backfire, near-broadside, and endfire frequencies, respectively, where $SPL = 20\log|p|$. The dashed arrows in Figs. 4(a)–4(f) indicate the radiation direction as calculated at each frequency using the circuit analysis described by Eq. (5).

Figures 4(d)–4(f) shows the measured sound pressure level radiated from an eight-cell LWA with materials and geometries equivalent to those used in the simulations. The structure was mounted in a $6 \times 6 \times 4\,m^3$ room on a frame such that the bottom of the LWA was 1 m off of the floor. Incident waves were generated using a piezoelectric piston transducer mounted at the end of the waveguide below the LWA in ten-cycle pulses over the frequencies of interest. The end of the waveguide opposite the sound source was loaded with absorptive foam to minimize interference of reflected waves inside the waveguide. The radiation pattern was measured using a microphone (B and K Type 4189) mounted on a three-axis positioning system. The bottom of the LWA structure was 0.29 m from the scanning origin (see Fig. 4) in the z-direction and 0.055 m from the structure in the r-direction.

Measurements were taken over an area of 1 m by 1 m at a spatial resolution of 0.05 m. Since the structure is axisymmetric, measurements were taken in a two-dimensional area in the r-z plane. The time-gated sound pressure level was

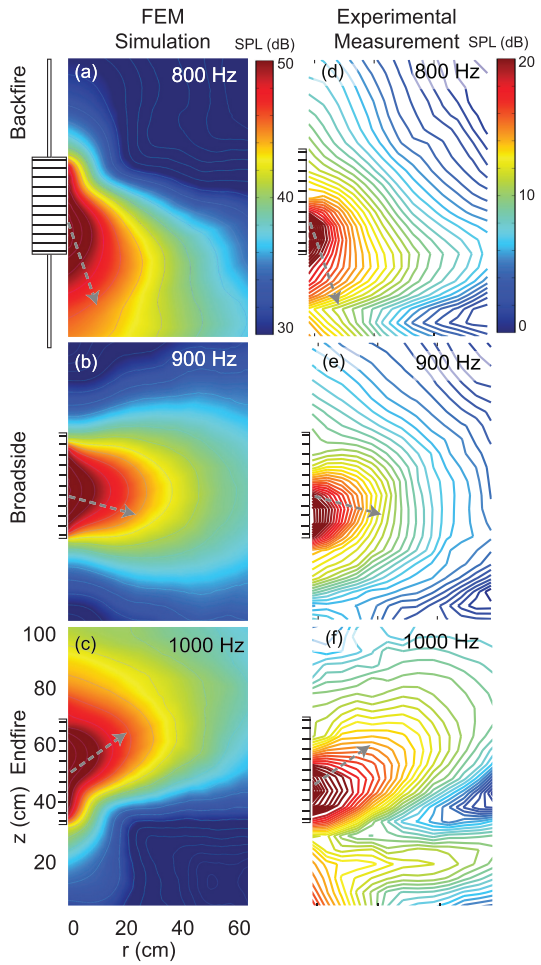

FIG. 4. Radiation profile next to the eight-cell LWA showing backfire behavior $f = 800$ Hz, showing near-broadside behavior $f = 900$ Hz, and showing endfire behavior $f = 1000$ Hz. Incident radiation is in the positive z-direction. (a)-(c) SPL obtained using finite element analysis. (d)-(f) Measured sound pressure level. Dashed gray arrows indicate the radiation direction as predicted using the acoustic circuit analysis.

calculated by averaging the measured pressure at a time after the cycle arrived at the microphone and before the arrival of reflected waves from the surfaces of the room.

Directional radiation behavior similar to that predicted with both the lumped parameter approach and FEM was achieved. As the incident frequency was increased, the directivity of the measured primary radiation lobe was observed to continuously progress from endfire to backfire radiation. No reduction in radiation was observed close to the transition frequency (broadside case), which suggests that the bandgap was closed achieving a matched condition between the positive and negative dispersion branches. Radiation angles predicted by the Bloch analysis (gray arrows in Fig. 4) provide a reasonable estimate of the directionality; however, the finite number of unit cells results in a wide beam-width making an exact assignment of directionality difficult based on the intensity maps alone. Increasing the number of unit cells in the antenna will result in a tighter beam pattern.

Side lobes were also observed in both the FEM prediction and measured radiation profile, the most prominent of which can be seen in the endfire case close to the scan origin [Figs. 4(c) and 4(f)]. Although the source speaker was insulated using absorptive foam, leakage from the source was not completely attenuated in the experimental case, which introduced source interference in the evaluated area closest to the source. This interference is evident as a decrease in the measured sound pressure level of the backfire case in the vicinity of the scan origin (near $z = 0$) compared to the FEM simulation. In the endfire case, distortion of the side lobe (which radiates toward the source) can be seen in Fig. 4(f). Fabrication imperfections, such as slight variations in the shunt width of different cells, may also result in a deviation from the ideal FEM radiation profile and directionality calculated from Eq. (5).

Experimental realization of an acoustic LWA that achieves a directed radiation beam pattern with the capability to continuously scan the radiation angle has been presented. Continuous scanning without a bandgap was achieved by matching the geometry conditions of the acoustic masses and compliances which made up the metamaterial substructure of the device. Excitation at frequencies below the zero-index frequency resulted in backfire radiation of the TL, while excitation above the zero-index frequency resulted in endfire radiation. The directionality of the measured beam pattern is well described by both acoustic circuit analysis of the idealized TL components and FEM of the as-fabricated prototype. This type of acoustic LWA has potential as either an acoustic source or acoustic sensor for detection of incident radiation angle. Additionally, by integrating active components into the structure, dynamic tuning of the propagation behavior could be possible.

Work was supported by the Office of Naval Research.

[1]X. Hu, K.-M. Ho, C. Chan, and J. Zi, Phys. Rev. B **77**, 172301 (2008).
[2]Z. Liu, X. Zhang, Y. Mao, Y. Zhu, Z. Yang, C. Chan, and P. Sheng, Science **289**, 1734 (2000).
[3]C. J. Naify, C. Chang, G. McKnight, and S. Nutt, J. Appl. Phys. **108**, 114905 (2010).
[4]J. Li and C. Chan, Phys. Rev. E **70**, 055602 (2004).
[5]S. Cummer and D. Schurig, New J. Phys. **9**, 45 (2007).
[6]H. Chen and C. Chan, Appl. Phys. Lett. **91**, 183518 (2007).
[7]T. Martin, M. Nicholas, G. J. Orris, L.-W. Cai, D. Torrent, and J. Sanchez-Dehesa, Appl. Phys. Lett. **97**, 113503 (2010).
[8]T. Martin, C. Layman, K. Morre, and G. Orris, Phys. Rev. B **85**, 161103 (2012).
[9]G. Eleftheriades, A. Iyer, and P. Kremer, IEEE Trans. Microwave Theory Tech. **50**, 2702 (2002).
[10]D. Jackson, C. Caloz, and T. Itoh, Proc. IEEE **100**, 2194 (2012).
[11]A. Lai, C. Caloz, and T. Itoh, IEEE Microw. Mag. **5**, 34 (2004).
[12]C. Cloz and T. Itoh, IEEE Microw. Wirel. Compon. Lett. **14**, 274 (2004).
[13]L. Liu, C. Cloz, and T. Itoh, Electron. Lett. **38**, 1414 (2002).
[14]F. Bongard, H. Lissek, and J. R. Mosig, Phys. Rev. B **82**, 094306 (2010).
[15]A. Moreau, H. Lissek, and F. Bongard, in Proceedings of the COMSOL Conference, Paris, France, 17–19 November 2010.
[16]C. Park, J. Park, S. Lee, Y. Seo, C. Kim, and S. Lee, Phys. Rev. Lett. **107**, 194301 (2011).
[17]S. Lee, C. Park, Y. Seo, Z. Wang, and C. Kim, J. Phys.: Condens. Matter **21**, 175704 (2009).
[18]Y. Seo, J. Park, S. Lee, C. Park, C. Kim, and S. Lee, J. Appl. Phys. **111**, 023504 (2012).
[19]S. Lee, C. Park, Y. Seo, Z. Wang, and C. Kim, Phys. Lett. A **373**, 4464 (2009).
[20]S. Lee, C. Park, Y. Seo, Z. Wang, and C. Kim, Phys. Rev. Lett. **104**, 054301 (2010).
[21]Y. Cheng, J. Xu, and X. Liu, Phys. Rev. B **77**, 045134 (2008).
[22]F. Bongard, "Contribution to characterization techniques for practical metamaterials and microwave applications," Ph.D. dissertation (Ecole Polytechnique Federale de Lausanne, 2009).